Nanoimprinted 2D-chiral perovskite nanocrystal metasurfaces for circularly polarized photoluminescence

Jose Mendoza-Carreño[1⊥], Pau Molet[1⊥], Clara Otero-Martínez[2], Maria Isabel Alonso[1], Lakshminarayana Polavarapu[2] and Agustín Mihi[1]*

1 Institute of Materials Science of Barcelona ICMAB-CSIC, Campus UAB Bellaterra 08193, Spain

2 CINBIO Universidad de Vigo, Materials Chemistry and Physics Group. Department of Physical Chemistry. Campus Universitario Lagoas-Marcosende, Vigo 36310, Spain

⊥ equal contribution

* E-mail: amihi@icmab.es

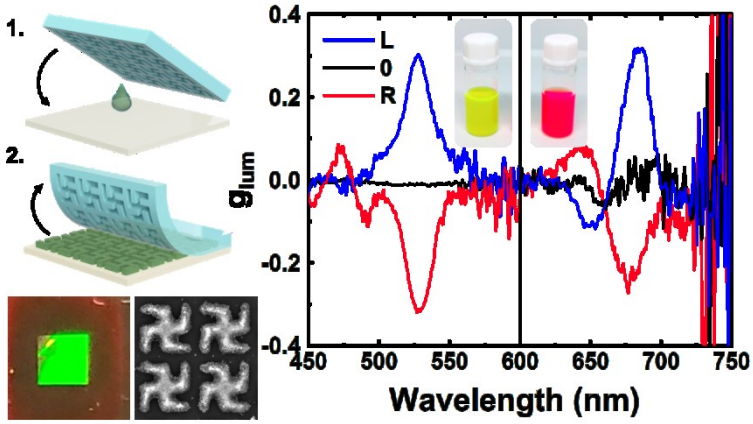

Keywords: Circularly polarized photoluminescence, chirality, nanoimprinting

The versatile hybrid perovskite nanocrystals are one of the most promising materials for optoelectronics in virtue of their tunable bandgaps and high photoluminescence quantum yields. However, their inherent crystalline chemical structure limits the chiroptical properties achievable with the material. The production of chiral perovskites has become an active field of research for its promising applications in optics, chemistry or biology. Typically, chiral halide perovskites are obtained by the incorporation of different chiral moieties in the material. Unfortunately, these chemically modified perovskites have demonstrated moderate values of chiral photoluminescence so far. Here we introduce a general and scalable approach to produce chiral photoluminescence from arbitrary nano-emitters assembled into 2D-chiral metasurfaces. The fabrication via nanoimprinting lithography employs elastomeric molds engraved with chiral motifs covering millimeter areas that are used to pattern two types of unmodified colloidal perovskite nanocrystal inks: green-emissive $CsPbBr_3$ and red-emissive $CsPbBr_1I_2$. The perovskite 2D-metasurfaces exhibit remarkable photoluminescence dissymmetry factors (g_{lum}) of 0.16 that can be further improved up to g_{lum} of 0.3 by adding a high refractive index coating on the metasurfaces. This scalable approach to produce chiral photoluminescent thin films paves

This article has been accepted for publication and undergone full peer review but has not been through the copyediting, typesetting, pagination and proofreading process, which may lead to differences between this version and the Version of Record. Please cite this article as doi: 10.1002/adma.202210477.

the way for the seamless production of bright chiral light sources for upcoming optoelectronic applications.

1. Introduction

Circularly polarized (CP) light is used in a vast number of photonic technologies, including 3D-imaging[1,2], biosensing[3,4], bioimaging[5], photocatalysts for asymmetrical synthesis[6,7], encrypted transmission[8] and spintronics[9], photoelectric devices and chiroptical materials. Traditionally, circularly polarized light is produced from unpolarized light by a combination of linear polarizers and quarter wave-plates or phase-shifting mirrors. These optical components limit device miniaturization, high-speed operation and cause severe brightness losses due to undesired light trapping. Said limitations can be overcome with the use of luminescent chiral materials. Unfortunately, chiral light emitters are very scarce in nature and resorting to chemical modification of existing luminescent materials is a challenging task that has resulted in limited fractions of circularly polarized luminescence (CPL) so far[10].

Over the last few years, halide perovskite nanocrystals (NCs) have emerged as one of the most efficient materials for optoelectronics because of a high photoluminescence (PL) quantum yield, tunable emission across the entire visible spectrum, and highly scalable colloidal synthesis[11–13]. The defect-tolerant nature of bromide and iodide halide perovskites enables the high PL quantum yield without the need of high bandgap passivation shells on their surfaces[14,15]. The ambitious next step in the development of metal halide perovskites is to endow them with chiral properties[16]. To this end, the synthetic versatility of metal halide perovskites is exploited for the incorporation of chiral organic molecules, either a bulky organic chiral cation inside the perovskite structure[17], a chiral molecule embedded between the layers of 2D-perovskites[9,18,19] or a chiral capping ligand in NCs[20]. Despite great efforts, chemical modification has provided limited values of CPL[21] at room temperature with g_{lum} values on the order of 10^{-3} which are insufficient for practical applications[21]. The luminescence dissymmetry factor g_{lum} quantifies the fraction of circularly polarized light emitted for each (right and left) handedness and it is defined as:

$$g_{lum} = 2\frac{(I_{L-CP} - I_{R-CP})}{(I_{L-CP} + I_{R-CP})} \quad (1)$$

where $I_{L\text{-}CP}$ and $I_{R\text{-}CP}$ are the emitted photoluminescence intensity for left circularly polarized (L-CP) and right circularly polarized (R-CP) light, respectively. It is worth noting that g_{lum} refers to PL and should not be confused with another typical magnitude used in the characterization of chiral materials, the dissymmetry factor (g), which quantifies the amount of each polarization that is absorbed by the material (also known as circular dichroism, CD). A clear description of each magnitude can be found in **Supporting Information S1**.

Alternative strategies to chemical or structural modification of the perovskites include the co-assembly of achiral perovskites with a chiral gelator to obtain a chiral arrangement[22], the injection of spin-polarized charge carriers[23], or directly encapsulating the materials within a liquid crystals acting as a polarization filter[24]. In addition, it is also possible to engineer the optical response of the perovskites to obtain CP light by coupling them to a photonic architecture that exhibits a chiral behaviour[25–27].

Similar approaches have been previously applied in semiconductors such as Galium Nitride nanolasers[28], InAs quantum dots (QDs) [29,30] as well as the coupling between plasmonic chiral metasurfaces with colloidal CdSe/ZnS QDs[31] to produce high fractions of CPL thanks to specific chiral electromagnetic (EM) modes with high dissymmetry factors. One way to endow chiral properties to an emitter is to place it in the vicinity of a chiral metasurface, where chirality is transferred from the external photonic architecture to the light source via resonant coupling. A different approach free from the introduction of external elements is to directly arrange the emitters into a chiral object capable of sustaining chiral resonances that affect the light produced from the constituting emitters. In the case of in $MAPbI_3$, the transference of chirality from a nanostructure engraved in the material by electron beam lithography resulted in a remarkable circular dichroism (CD), a differential light absorption for each circular polarization[32] but no chiral photoluminescence was reported therein. In the case of perovskite NCs, inorganic silica right (or left) handed nanohelices have been used as chiral templates to induce optically active properties to $CsPbBr_3$ NCs grafted on their surfaces, reaching maximum g_{lum} values of 6.9×10^{-3} at 517.5 nm[33]. Resorting to nanophotonic structures is promising alternative to induce a chiral character in any active media[25,27], however it comes with several setbacks such as the cumbersome lithographic steps (especially if chiral objects are to be designed) or the typically small areas fabricated which undermine their implementation in actual applications.

Nanoimprinting lithography is an exciting alternative for the fabrication of nanostructures with high resolution, while being scalable, low cost and free of cleanroom restrictions[34–36]. Nanoimprinting lithography uses pre-patterned molds to induce the ordering of a colloidal material such as perovskite NCs without recurring to etching processes nor external scaffolds via a template-induced self-assembling process[37]. This soft lithography derived approach has been previously applied to generate periodic arrangements of colloidal gold nanoparticles[38], PbTe nanocrystals[39] and colloidal perovskite NCs[40] to control and enhance their optical properties through lattice-related plasmonic/photonic resonances.

In this work, we demonstrate the fabrication of large area CPL-active 2D-chiral perovskite-metasurfaces by template-induced self-assembly of halide perovskite NCs using pre-patterned elastomeric stamps. Two types of non-chiral perovskite inks, green-emissive $CsPbBr_3$ and red-emissive $CsPbBr_1I_2$ NCs are used to obtain color tunable CP light. The single-step fabricated perovskite 2D-chiral metasurfaces exhibit CP PL with a maximum g_{lum} of 0.16 at RT within the visible region. These g_{lum} values increase up to 0.31 for both perovskite inks by coating the metasurfaces with a high refractive index titanium dioxide (TiO_2) layer that increases the light extraction efficiency. In addition, each side of the 2D-chiral metasurface emits light with opposed handedness, a characteristic inherited from the photonic behavior from the metasurface. The CPL collected from each side of the metasurface is analyzed and explained via numerical simulations of the chiral near-fields present in the architectures. Our results underpin template induced self-assembly as a versatile and scalable technique that enables control on the optical properties of the nanostructured inks.

2. Results and discussion

Two types of perovskite nanocube inks ($CsPbBr_3$ and $CsPbBr_1I_2$ NCs) were synthesized by ligand-assisted tip-ultrasonication and halide exchange (**Figure S2**). The $CsPbBr_3$ NCs, exhibit green PL with a peak maximum at 519 nm (**Figure 1a**), while the $CsPbBr_1I_2$ NCs emit red PL with a peak maximum at 645 nm (**Figure 1b**). The prepared $CsPbBr_3$ and $CsPbBr_1I_2$ NCs are nearly-monodisperse with average size of 10.7 nm and 12 nm, respectively (**Figure S2**). Both colloidal dispersions were purified by centrifugation to obtain NC inks in hexane at a 20 mg/mL and 80 mg/mL concentration for green and

red NCs, respectively. The CPL-active chiral nanostructures were fabricated via template-induced self-assembly of halide perovskite NC inks using 3 different pre-patterned polydimethylsiloxane (PDMS) molds with 500 nm gammadion-like structures (9 mm^2 patterned areas) with left (L), right (R) and racemic (O) orientations in a square array with a periodicity of 600 nm (structure dimensions in **Figure 1c**). The gammadion geometry was chosen mainly due to the abundance of previous literature[28–30,32,41,42,42–46], which facilitates the comparison between the optical properties of the newly produced nanostructures by nanoimprinting lithography and previous results from structures produced by electronic lithography. Secondly, the C4 symmetry of the array helps minimizing the contribution to the PL from linearly polarized light which results in elliptical polarization. Finally, the gammadion was one of the simplest geometries that could be used for template-induced self-assembly exhibiting a chiral character with a 4-fold symmetry (a more detailed explanation of this choice in geometry can be found in **Supporting Information 3**).

The fabrication process, summarized in **Figure 1d**, begins with 0.7 µL of the colloidal solution deposited on a cleaned glass coverslip and immediately covered with the pre-patterned stamp. After the solvent is evaporated (5 min), the stamp is removed, leaving the nanostructured perovskite NC film behind. The high quality of the resulting perovskite 2D-chiral metasurfaces with R (clockwise orientation), L (counter-clockwise orientation) and O (racemic mixture of R and L gammadions) enantiomers was confirmed through SEM imaging (**Figure 1e-g**, **Figure S3**) in which the constituent perovskite nanocubes can be distinguished (**Figure 1h**). The racemic pattern acts as control to ensure that the origin of the optical chiral properties arise from the specific enantiomeric features of the metasurface.

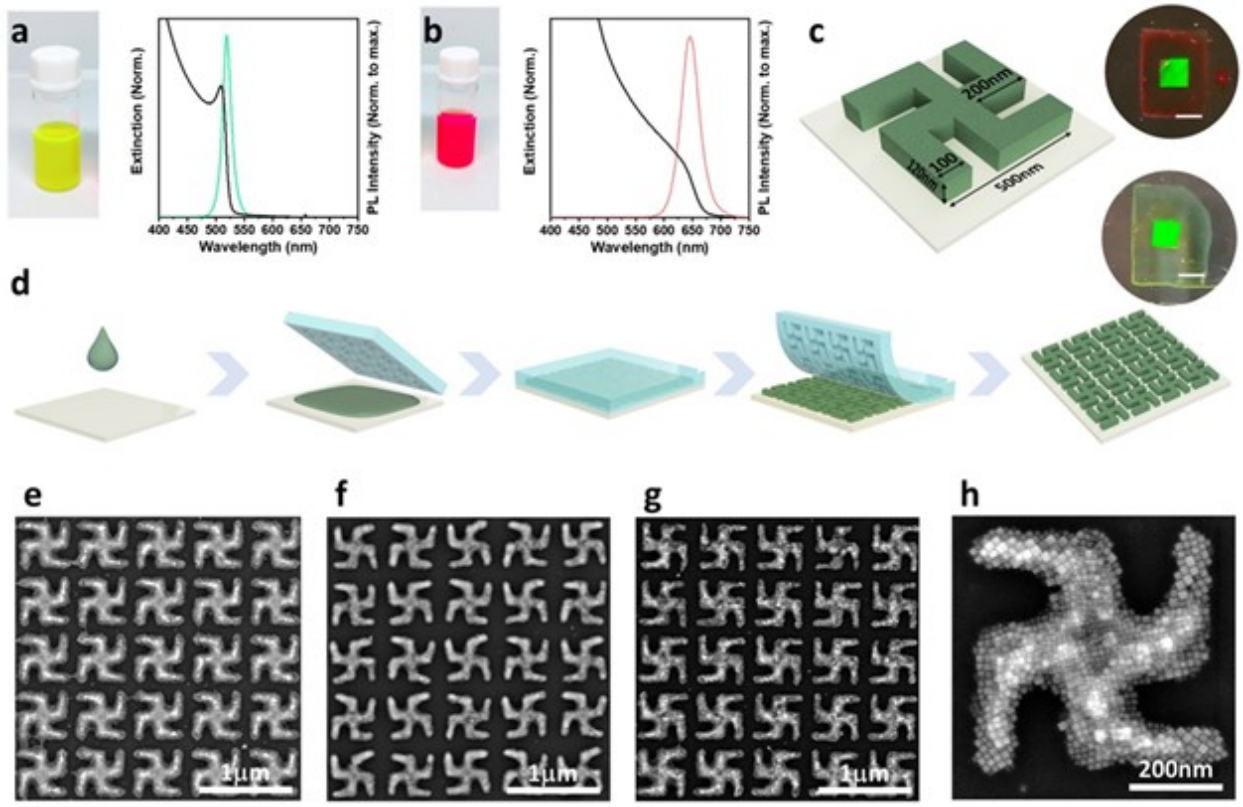

Figure 1. *Fabrication of the 2D-chiral metasurface. Photograph of the original colloidal dispersion, extinction and PL intensity spectra of green $CsPbBr_3$ NCs (**a**) and red $CsPbBr_1I_2$ NCs (**b**). (**c**) Schematic of the chiral unit. Inset photographs of the actual samples of red $CsPbBr_1I_2$ NCs (top) and green*

*$CsPbBr_3$ NCs (bottom) large area 2D-chiral metasurfaces with a scale bar = 3 mm. **(d)** Schematic illustration of the fabrication process of 2D-chiral metasurfaces by the templated-assembly technique. Scanning electron microscope (SEM) images of L-Gammadion **(e)**, O- racemic **(f)** and R-Gammadion **(g)** metasurfaces. **(h)** Large magnification SEM of an L-Gammadion unit composed by $CsPbBr_3$ perovskite NCs.*

One of the key properties of 2D-chiral metasurfaces is the inversion symmetry[25,29,30,47]. Unlike 3D-chiral objects such as helices, the gammadion shapes are considered to be 2D-chiral, meaning that the handedness of the object changes when inspected from the top or from the bottom[42,43]. This change in chiroptical response is corroborated by the chiral near-fields with opposed handedness appearing at each side of the structure when light impinges from one or the other side as illustrated in **Figure 2**. To evaluate the intrinsic chirality of the resulting perovskite 2D-chiral metasurfaces and their electromagnetic near-fields[48] at each side of the gammadion, we resort to the optical chirality factor C. This magnitude is defined as:

$$C = -\frac{1}{2}\varepsilon_0 \omega \, Im\{\vec{E}^*(\vec{r}) \cdot \vec{B}(\vec{r})\} \quad (2)$$

where ε_0 is the vacuum dielectric permittivity, ω is the angular frequency of the EM wave, $\vec{E}^*$ is the conjugated electric field and $\vec{B}$ is the magnetic field. This optical chirality factor is often normalized to the reference value. In this work, the optical chirality factor is normalized to the R-CP light in vacuum as follows (more details in **Supplementary Information 5**):

$$\hat{C}(\lambda,\vec{r}) = \frac{C_{structure}(\lambda,\vec{r})}{C_{vacuum}^{RCP}} = -\frac{\mu_0 c}{2E_0^2} Im\{\vec{E}^*(\lambda,\vec{r}) \cdot \vec{H}(\lambda,\vec{r})\} \quad (3)$$

As the normalization is carried out using R-CP, the sign of the magnitude denotes the handedness of the polarization state of light, i.e. positive values of $\hat{C}$ denote predominant R-CP, whereas negative ones correspond to higher contribution of L-CP light. All the normalized $\hat{C}$ values presented herein are evaluated using **Equation 3**. The values of $\hat{C}$ vary from -1 for perfectly L-CP light up to 1 for R-CP light. Near-field values of $|\hat{C}| > 1$ are considered to be super-chiral[49,50] and can be found in our structure when directly illuminated with CP light (**Figure S4-7**). Near-field values of $|\hat{C}| > 1$ imply that the electromagnetic near-field distribution shows a greater optical chirality than a perfectly circularly polarized plane wave. However, the aim of this work is to understand how the gammadion geometry can transfer its structural chirality to unpolarized light (with original $\hat{C} = 0$), when a beam impinges from outside or when the light is emitted within the structure, rendering values of $\hat{C} \neq 0$ (**Figure 2**).

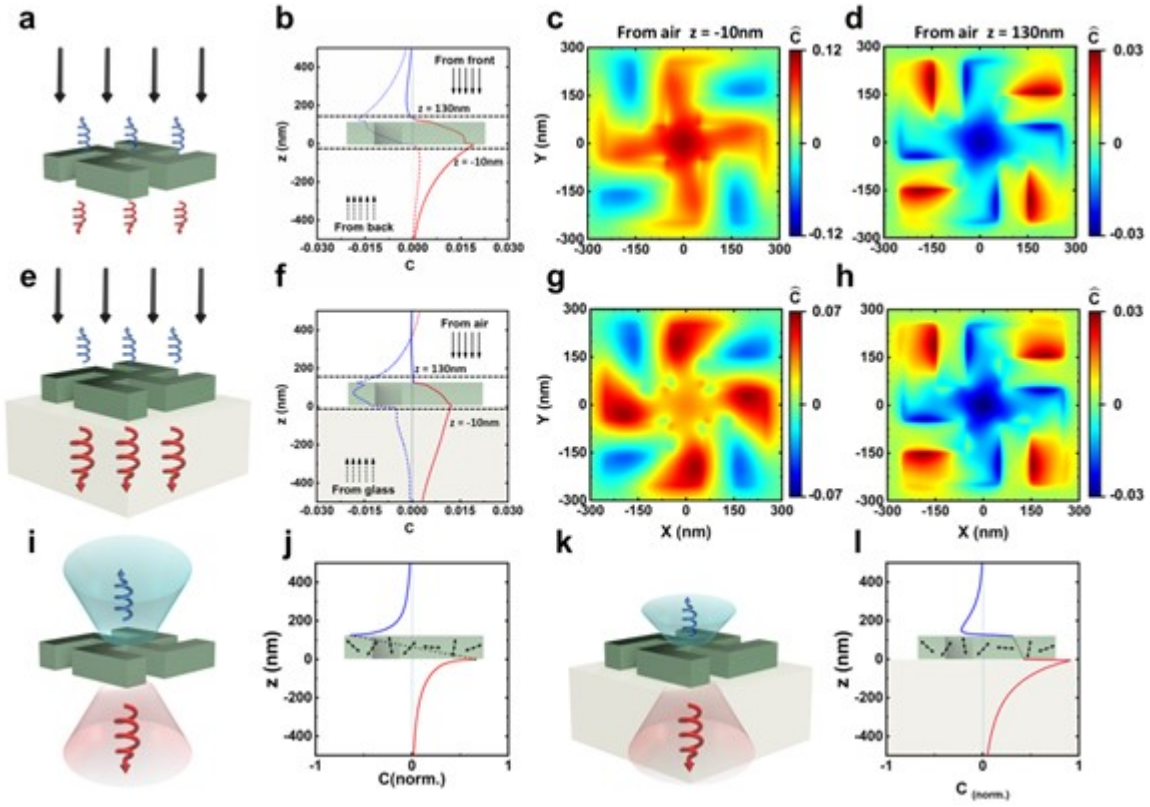

Figure 2. *Optical chirality C inversion and dissymmetry for both sides of L-Gammadion at the emission wavelength (520 nm). Schematic illustration of an L-Gammadion transferring optical chirality to unpolarized light and the calculated optical chirality factor along the propagation axis for a system with (**a**,**b**, **first row**) and without (**e**,**f**, **second row**) inversion symmetry along the axis. Local optical chirality factor in the symmetric and non-symmetric system at 10 nm distance from the gammadion unit for the transmitted (z=130 nm **c**,**g**) and reflected (z=-10 nm **d**,**h**) light. (**i**) Schematic illustration of an L-Gammadion emitting both polarizations for a system with (**i**) and without (**k**) inversion symmetry along the axis depending on the surface of emission measurement. Normalized optical chirality factor computed by FDTD simulations for randomly out of phase dipole cloud placed within the L-gammadion volume polarizations for a system with (**j**) and without (**l**) inversion symmetry*

When unpolarized light propagating in z<0 direction impinges on a single L-gammadion structure suspended in air placed between z = 0 and z = 120 nm (**Figure 2a**), the integrated $\hat{C}$ factor along the propagation direction of the wave changes its value from negative (L-CP) to positive (R-CP) as it travels through the gammadion (**Figure 2b**, solid line). The simulated spatial distribution of the near-field in an XY plane for the reflected wave located 10 nm above (z=130 nm, **Figure 2c**) or for the transmitted wave below (z=-10 nm, **Figure 2d**) the L-Gammadion shows opposite values of $\hat{C}$ factor, illustrating the symmetry inversion in these 2D metasurfaces. The $\hat{C}$ factors are reversed when the light impinges from the bottom to z>0, hence effectively encountering an R- gammadion (**Figure 2b**, dashed line). For a given propagation direction, the dissymmetry observed in $\hat{C}$ at each side of the structure is only due to its higher transmittance coefficient compared to less intense reflected EM fields. The presence of the substrate in our experiments generates a refractive index mismatch between the air (n=1) and the glass (**Figure 2e**) therefore breaking the symmetry inversion of the system[27,42,43]. This asymmetry in surrounding media effectively results in a quasi-2D chiral system in which different magnitudes of $\hat{C}$ factor are found on each side of the structure, as observed comparing **Figures 2a-d and 2e-h**.

Next, we considered the situation in which the light is generated within the gammadion, in an attempt to predict qualitatively the effects of the nanostructuration on the PL from the perovskites. We calculated the values of $\hat{C}$ at each side of the structure for light produced from a series of randomly oriented out-of-phase dipoles placed within the L-gammadion volume. In the case of an L-gammadion suspended in air (**Figure 2i**,**j**), the FDTD simulation shows opposite values of the chirality factor $\hat{C}$ on each side of the structure. As a result, an L-gammadion metasurface surrounded by air preferentially emits L-CP light towards the upper side and R-CP towards the bottom side with the same intensity and specificity (**Figure 2j**). The presence of a glass substrate affects the 2D-chiral emission character of the gammadion, as presented in **Figure 2k**,**l**[42,43]. Opposite handedness is still observed at each side of the L-gammadion, but the refractive index mismatch renders higher $\hat{C}$ values on the glass side (**Figure 2k**,**l**). This analysis indicates that a full optical characterization of the CPL from the 2D metasurfaces must consider light emitted from both sides of the structure, where higher luminescence dissymmetry factor g_{lum} is expected for light emitted on the glass side.

We move now to the experimental characterization of the metasurfaces. Photoluminescence from L-, O- and R- metasurfaces made from $CsPbBr_3$ NCs was collected from both the air and the glass sides and the results presented in **Figure 3**. A complete description of the optical setup used to optically characterize each side of the 2D-chiral metasurfaces along with flat thin films (used as controls) made from both types of perovskite inks can be found in the **Experimental section**. As predicted by the simulations in **Figure 2**, CPL with opposite handedness is preferably generated from each side of the metasurface but with a higher chiral dissymmetry factor value at the glass side. When measured from the air side, L- and R- gammadion metasurfaces displayed L-CP and R-CP preferential emissions with maximum g_{lum} values of 0.06 and -0.04, respectively. Instead, glass side measurements of L and R enantiomeric surfaces displayed R-CP and L-CP preferential emissions respectively with maximum g_{lum} values of -0.12 and 0.16. As expected, no selective CPL was displayed by the racemic mixtures (**Figure 2b**, **f**) nor unpatterned NCs films (**Figure S12a**) indicating that the CPL observed is originated by the chiral metasurface geometry. The values of polarized PL (g_{lum}) obtained in our metasurfaces represent a remarkable enhancement of 2 orders of magnitude over most previous works in perovskite only thin films (g_{lum} around 10^{-3})[21].

The experimental and FDTD simulated circular dichroism CD of the metasurfaces (**Figure S9**), reported CD values of $\Delta T/T=\pm 0.005$ at the emission wavelength of 520 nm for both enantiomeric $CsPbBr_3$ metasurfaces while no $\Delta T/T$ was observed from the racemic sample (**Figure S11**).

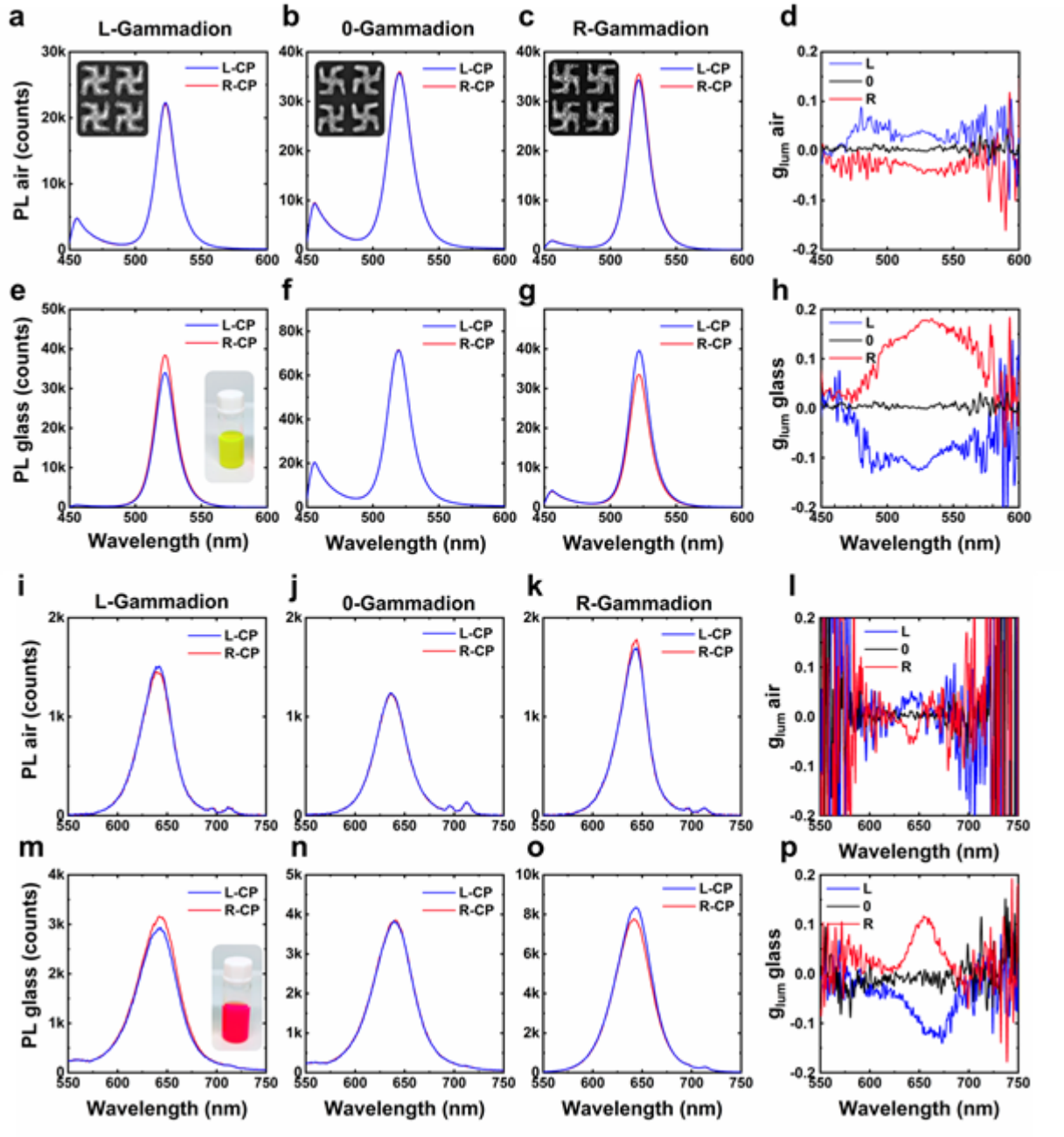

Figure 3. *Chiral PL of green $CsPbBr_3$ NCs and red $CsPbBr_1I_2$ perovskite NC. PL spectra measured from air (first row) and from the glass (second row) for green $CsPbBr_3$ NCs metasurfaces of L-Gammadions (**a**,**e**), racemic mixture (**b**,**f**) and R-Gammadions (**c**,**g**). g_{lum} of metasurfaces comprising L-Gammadions (blue), R-Gammadions (red) and racemic mixture (black) from air (**d**) and from glass (**h**). PL measurements from air (third row) and from the glass (forth row) for red $CsPbBr_1I_2$ NCs metasurfaces of L-Gammadion (**i**,**m**), racemic mixture (**j**,**n**) and R-Gammadion (**k**,**o**). (**l**,**p**) g_{lum} for metasurfaces of the L-Gammadion (red), racemic mixture (black) and R-Gammadion (blue).*

Producing circularly polarized photoluminescence via chiral shape patterning, opens up novel opportunities to obtain CPL from a variety of nano-emitters. To illustrate the versatility of our fabrication procedure, we fabricated chiral metasurfaces using a different perovskite NC ink with composition $CsPbBr_1I_2$, hence moving to the red part of the visible spectrum. In the last two rows of **Figure 3** we present the chiral PL obtained from the metasurfaces made from $CsPbBr_1I_2$ NCs inks with

a maximum emission at 645 nm (**Figure 1**). $CsPbBr_1I_2$ NCs gammadion arrays reached maximum g_{lum} values of -0.13 and 0.12 when measured from the glass substrate for the L and R enantiomers respectively (**Figure 3m**, **o** and **p**). Similarly to the green $CsPbBr_3$ NCs, CPL from the air side was lower that from the glass side, reaching values of g_{lum}=±0.04 (**Figure 3i,k** and **l**). There was no selective CPL displayed by neither racemic mixtures (**Figure 3j**,**n**) nor unpatterned NCs films (**Figure S12b**). The versatility presented herein paves the way to fabricate CP-active halide perovskite NCs chiral structures directly with unmodified or intrinsically achiral perovskites NCs, such as the ones proposed by Joseph M. Luther and D. H. Waldeck among others[20,51], and can be extended to wide variety of nanometric colloidal emitters.

At this point, we believe that the values of g_{lum} obtained in our metasurfaces are limited by several structural factors such as: feature height (120 nm), geometry of the chiral motifs and refractive index of the $CsPbBr_3$ and $CsPbBr_1I_2$ nanocrystals (in our simulations comprised between 1.7 and 2, as obtained by ellipsometry and modelled with modified harmonic oscillators[52], see **Supplementary Information 6**). New designs of chiral geometries supporting stronger chiral resonances or the use of active materials with higher refractive index would definitely increase the optical chirality fields sustained by the metasurface, thus increasing the fraction of CPL produced. To illustrate this later point, we simply coated the previously studied perovskite metasurfaces with a high refractive index coating (TiO_2). High refractive index materials have been widely used to maximize the light matter interaction in optically active nanostructures[53–55], as it is possible to achieve strong electromagnetic resonances avoiding the optical losses presented by their homologue plasmonic counterparts[56,57]. Here, we thermally evaporated 75 nm of TiO_2, a high refractive index material with n = 2.4 and no absorption in the visible range, onto the perovskite metasurfaces. The effects of the TiO_2 coating on the $CsPbBr_3$ metasurfaces are shown in **Figure 4**. Higher g_{lum} values are obtained at the peak emission wavelength, going up to 0.31 when measured from the air side of the metasurfaces, reaching also values of 0.1 when inspected from the substrate side (**Figure 4e**). Now, the highest values of CPL are obtained from the air side, where the higher refractive index coating helps the light extraction from the metasurface for both perovskite compositions (**Figure 4b**, **d**, and in **Figure S14)**. The preferential CPL from the air side of the titania coated metasurface correlates well with predicted $\hat{C}$ by FDTD simulations shown in **Figure 4c** calculated from a random distribution of dipoles as in **Figure 2h**. Therefore, the TiO_2 layer renders our metasurface with PL emissions with higher CP selectivity and g_{lum} factors to the air side. This result serves as an example of how the specific CPL and directionality can be effectively tuned by designing the specific layers composing the 2D-chiral metasurface, paving the way for further values of g_{lum}.

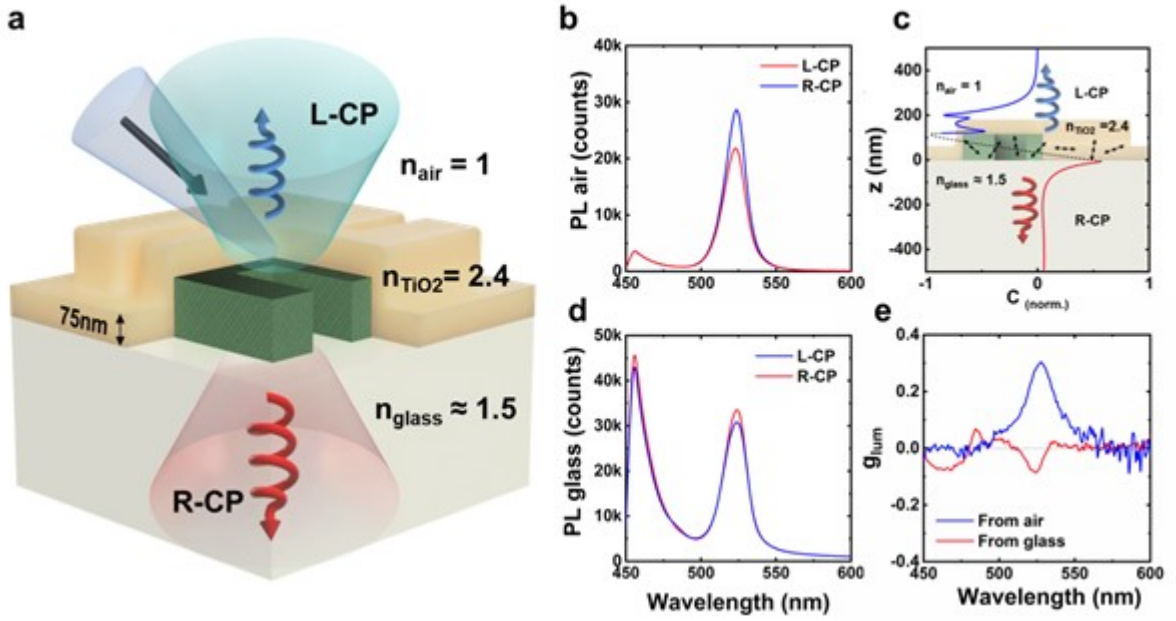

Figure 4. *Chiral dissymmetry PL emission from the 2D-chiral metasurface coated with 75 nm of TiO_2. (**a**) Schematic illustration for the excitation of a high refractive index TiO_2 coated L-Gammadion emitting preferentially L- or R-PL on each side of the metasurface. Chiral PL measurement of L-CP (blue) and R-CP (red) measured from the (**b**) air and (**d**) glass side. (**c**) Normalized optical chirality factor computed by FDTD simulations for a randomly out-of-phase dipole cloud placed within perovskite L-gammadion volume. (**e**) Comparison of the g_{lum} measured through the air (blue) and the glass (red) side.*

The TiO_2 coated gammadion metasurfaces show sharper and more pronounced extinction peaks, a dramatic increase in the transmission CD compared to the original nanostructured array and finally, stronger chiral emission. In **Figure 5** we summarize the transmission CD and CPL measurements for the titania coated gammadions fabricated with green $CsPbBr_3$ (**Figure 5a-h**) and red $CsPbBr_1I_2$ NCs (**Figure 5i-p**). In this case both the CD and PL experiments were performed impinging light from the glass side as now emitted light is preferentially out-coupled from the air side with the TiO_2. Therefore, L-gammadions display preferential L-CP emission and R-gammadions preferential R-CP emission. In both NCs, $\Delta T/T$ and g_{lum} values present a strong spectral correlation.

For green $CsPbBr_3$ NCs, experimental circular dichroism values of $\Delta T/T$=0.07 were obtained at the emission wavelength of λ=520 nm (**Figure 5a-d, Figure S17**), being twelve times higher than the ones displayed by metasurfaces without TiO_2 coating in **Figure S11**. In addition, highly preferential CPL was shown for both enantiomers, reaching g_{lum} values of ±0.31 (**Figure 5e-h**). Similar CD results were obtained with red $CsPbBr_1I_2$ NCs, reaching maximum $\Delta T/T$ values of 0.042 (**Figure 5i-l, Figure S17**). Interestingly, in this case there is a strong inversion in the handedness behavior of the structure due to a lattice resonance supported by the gammadion array (of 600 nm period) which in this case overlaps with the emission band of the $CsPbBr_1I_2$ NCs (**Figure S16**). Therefore, the R-gammadion array (**Figure 5o**) shows both a maximum R-CP preferential emission at 645 nm with g_{lum} values of +0.1 and a maximum of L-CP preferential emission at 680 nm with g_{lum} values of -0.30 (**Figure 5m-p**). This last result encourages the use of lattice resonances supported by chiral motif arrays to further improve the optical chirality values of a metasurface[58].

The high g_{lum} values obtained for both types of perovskite nanocrystals illustrate the versatility of our approach to produce CPL from an unmodified achiral emitter. NCs chiral structures can be complemented and enhanced with the seamless addition of high refractive index materials on the structure. This leads to the conclusion that with a rational design on the chiral nanostructure, the materials composing it and targeting one specific emission wavelength (more details in **Supplementary Information 9**), one can obtain even higher g_{lum} values with template-induced self-assembly of halide perovskite NCs.

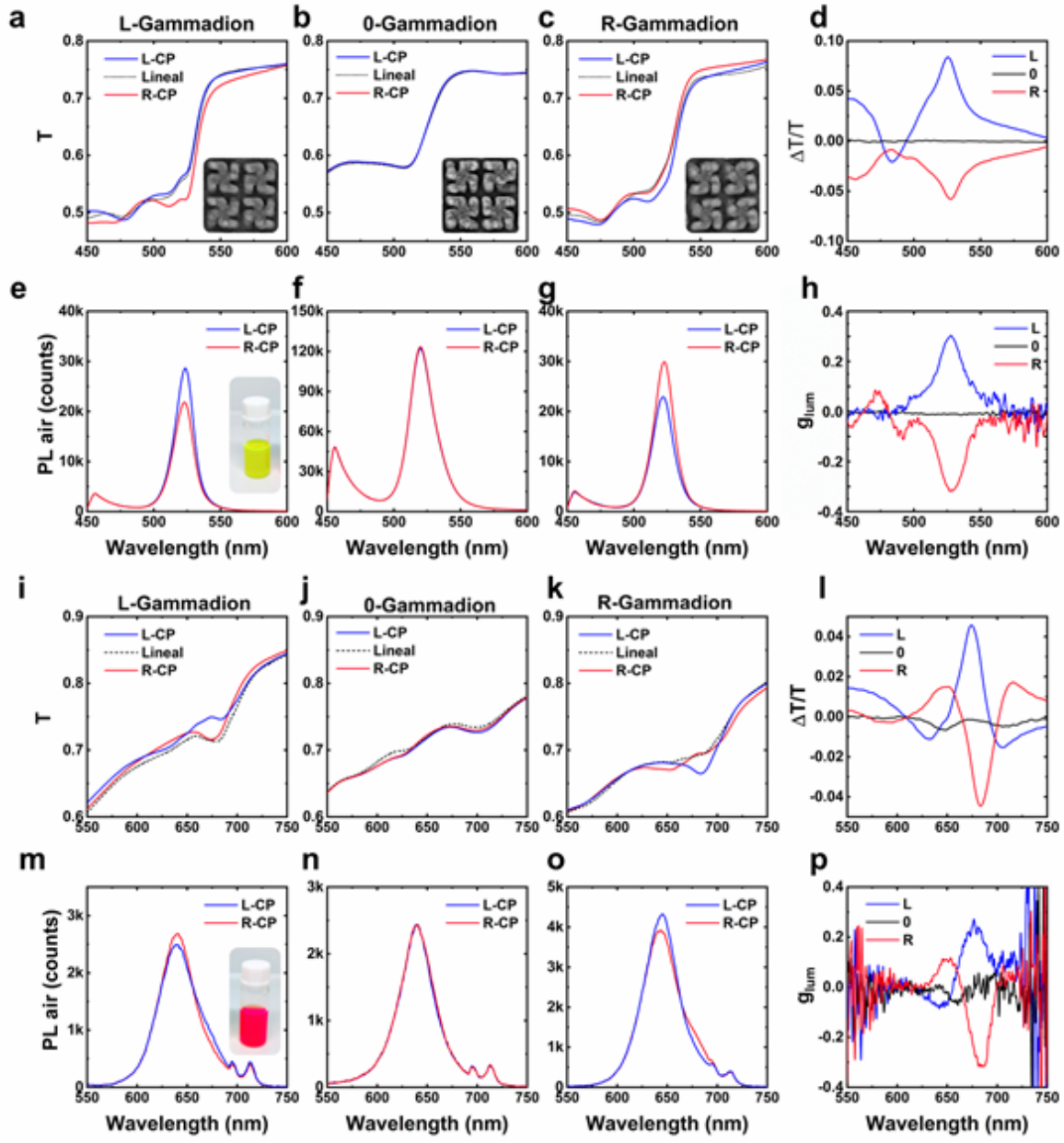

Figure 5. *Summary of CD and chiral PL for both high refractive index TiO_2 coated green $CsPbBr_3$ and red $CsPbBr_1I_2$ perovskite NC. Transmittance spectra (first row) and PL spectra (second row) for high refractive index TiO_2 coated green $CsPbBr_3$ NCs metasurfaces of L-Gammadion (**a**,**e**), racemic mixture (**b**,**f**) and R-Gammadion (**c**,**g**). CD (**d**) and g_{lum} (**h**) for L-Gammadion (blue), R-Gammadion (red) and racemic mixture (black). Transmittance spectra (third row) and PL spectra (fourth row) for high refractive index TiO_2 coated red $CsPbBr_1I_2$ NCs metasurfaces of L-Gammadion (**i**,**m**), racemic mixture*

*(**j**,**n**) and R-Gammadion (**k**,**o**). CD (**l**) and g_{lum} (**p**) for L-Gammadion (blue), R-Gammadion (red) and racemic mixture (black).*

3. Conclusions

In this work, we demonstrated large area CPL-active halide perovskite NCs chiral structures using template-induced self-assembly. We produced 2D-chiral metasurfaces by nanostructuring two types of non-chiral halide perovskite NCs, $CsPbBr_3$ and $CsPbBr_1I_2$ into gammadion arrays. This low cost and scalable fabrication approach can be seamlessly applied to other kind of emitters, including those with intrinsic chirality, to directly obtain circularly polarized light with relevant g_{lum} values. In this work, the fabricated 2D-chiral metasurfaces rendered the perovskite NCs with CPL selectivities reaching g_{lum} values up to 0.16 at RT. Opposed handedness CPL is observed at each side of the 2D chiral metasurface, which is corroborated numerically by analyzing the optical chirality of the near-fields generated at top and bottom sides of the structure in air or glass supported. Finally, we further improved the chiral emission properties of the metasurface by adding a thin film of a transparent high refractive index material atop. This coating rendered maximum g_{lum} factors of 0.31 and demonstrated the ability to design and optimize the preferential chiral response by engineering the layers composing the metasurface. We believe that the work presented herein will contribute to the development of large scale selective CPL sources with the most efficient common light emitters that can be combined with chemical modification to achieve even greater CPL values with great potential for displays and quantum technologies.

4. Experimental section

Materials

Cesium carbonate (Cs_2CO_3, 99,9%), lead (II) bromide ($PbBr_2$, >98%), lead (II) iodide (PbI_2, 99%), 1-octadecene (ODE, $C_{18}H_{36}$, 90%) oleic acid ($C_{18}H_{34}O_2$, 90%), and oleylamine ($C_{18}H_{37}N$, 70%) were purchased from Merck. Hellmanex III solution and Hexane solutions were purchased from Millipore-Sigma. Acetone, Isopropanol and NaOH was purchased from Labbox. Polydimethylsiloxane (PDMS, Sylgard 184) was purchased from Dow Corning (Michigan, USA). The hard PDMS (hPDMS) mixture kit was purchased from Gelest (USA). All chemicals were used as received.

Preparation of $CsPbBr_3$ and $CsPbBr_1I_2$ perovskite NCs

Synthesis of $CsPbBr_3$ perovskite NCs. In a typical synthesis, 15 mL of octadecene, 1.5 mL of oleic acid and 1.5 mL of oleylamine and the precursor powders (1 mmol of Cs_2CO_3 and 3 mmol of $PbBr_2$) were loaded in a 50 ml beaker. Then, the reaction medium was subjected to tip-ultrasonication (SONOPULS HD 3100, BANDELIN) at a power of 30 W for 30 minutes. During the course of reaction, the colour change of reaction mixture from colorless to yellow indicated the formation of perovskite NCs. The solution was purified by centrifugation (8000 rpm, 10 min) and the sediment was redispersed in 25 mL of hexane. Finally, the solution was centrifuged again (5000 rpm, 8 min) in order to remove the large particles. The supernatant was collected and used for the self-assembly as well as to obtain $CsPbBr_1I_2$ NCs by halide exchange using PbI_2 solution.

Preparation of the PbI_2 solution. 4 mmol of PbI_2, 4 mL of oleylamine, 4 mL oleic acid and 100 mL of hexane were loaded in a 250 ml Pyrex bottle. The solution was heated-up until 60 ºC under vigorous stirring until the salt was completely dissolved. The PbI_2 solution in hexane was employed as iodide source for the synthesis of $CsPbBr_1I_2$ perovskite NCs.

Synthesis of $CsPbBr_1I_2$ perovskite NCs. $CsPbBr_1I_2$ NCs were synthesized by halide exchange reaction. In a typical synthesis, 25 mL of the $CsPbBr_3$ NCs colloidal dispersion previously synthesized were loaded in a 250 ml Pyrex bottle. The solution was heated-up to 40 ºC and then PbI_2 solution was consecutively added under vigorous stirring until the PL tuned to 645 nm. The reaction was monitored by photoluminescence observing a red-shift in the PL emission that indicates the halide exchange.

Preparation of the Patterned stamps

Preparation of the original master structures. The original silicon masters (purchased from CONSCIENCE, Sweden) were constituted of arrays of gammadion shapes with 500 nm width, 120 nm depth, disposed in a squared arrangement forming a lattice of 600 nm pitch in 3 x 3 mm^2 areas. The masters were silanized with an anti-sticking layer of perfluorooctyl-trichlorosilane to prevent the adhesion of the silicones and resists during replication. The silanization took place through chemical vapor deposition, leaving the masters for 30 minutes in a desiccator under vacuum together with 4µL of perfluorooctyl-trichlorosilane. The substrates were rinsed with acetone and heated to 150 °C for 30 min to remove unreacted silane.

Preparation of the working masters: Intermediate masters are negative replicas of the original masters, used to obtain a final replica in PDMS of the original hole arrays. These negative hard molds were prepared using UV-nanoimprinting. Specifically, a drop of Ormostamp, a photosensitive resist, was placed directly on top of the silanized silicon master. Then, a cleaned glass slide was gently pressed on top making sure no bubbles remained trapped between the slide and the Ormostamp. The photoresist was then cross-linked and hardened under UV lamp for 5 minutes. To demold the Ormostamp working master, we placed the substrates on a hot plate at 160°C. The difference in thermal expansion between photoresist and silicon induced the detachment of the Ormostamp mold. Finally, the working masters were silanized using isopropanol as solvent instead of acetone, to avoid the detachment of the photoresist layer from the glass slide.

Preparation of the PDMS Molds: Hybrid hard/soft PDMS molds are needed to ensure the correct replica of the working masters avoiding structural collapsing during demolding. In particular, they are composite molds were the structured layer (with a thickness of few microns) is made of hard PDMS (hPDMS), while the backbone (several millimeters) is made of standard soft PDMS. To prepare the hPDMs mixture, 1.7 g of 7-8% vinylmethylsiloxane is mixed with 0.05 g of 1, 3, 5, 7 tetracetylcyclosilane, 9 µL of Pt catalyst, 0.5g of 25-35% hydroxyl siloxane, and 1.5 g of toluene in this order. All the additions need to take place under vigorous stirring. After 5 minutes of stirring, the obtained mixture can be used for approximately 20 min, before it solidifies after toluene evaporation. While it is still liquid, the mixture is drop casted onto the master and spread over the surface using an air gun. This step ensures that the mixture covers entirely all the structures and leaves no microbubbles trapped. After repeating this last step two or three times for each working master, the substrates are left 1h at room temperature to ensure complete evaporation of the toluene, and 1 more hour at 60°C to cure the hPDMS. Next, we prepared the backbone by standard PDMS protocols. A 10:1 mixture of the monomer and curing agent are mixed vigorously and left degassing for approximately an hour. Then,

the mixture is gently poured onto the samples with the cured hPDMS. Finally, the polymer is cured at 100°C for another hour. Once the PDMS is cured, it is manually demolded from the master.

Preparation of the colloidal nanoparticle assemblies: The various colloidal solutions of halide perovskite NCs were prepared for template induced self-assembly by centrifugation. Specifically, the solutions were cleaned from the excess surfactant by centrifuging at 15.000 rpm and concentrated in hexane 20 mg/mL and 80 mg/mL concentration for $CsPbBr_3$ and $CsPbBr_1I_2$, respectively.

Preparation of the substrates for the assembly: Borosilicate microscope coverslips (Menzel,#2) were used as substrates. The substrate preparation protocol comprised cleaning with sonication in acetone, Hellmanex III (3%) solution, isopropanol, and lastly a hydrophilization with NaOH for 10 min each step, with water rinsing in between.

Template induced assembly: Perovskite NC metasurfaces were prepared by depositing a 0.7 µL drop of halide perovskite NCs on top of a hydrophilized coverslip glass. The drop is then covered with a pre-patterned PDMS mold and left for 5 minutes. After drying, the mold is removed, leaving the perovskite nanostructured film on the coverslip substrate.

High refractive index coating: 75 nm of TiO_2 were deposited on top of the structured perovskite gammadions arrays by electron beam (e-beam) deposition (ATC-8E Orion from AJA International Inc. with up to 10 kV HV source).

Optical characterization.

UV-Vis and photoluminescence spectroscopy. UV-Vis extinction spectra were obtained using a Cary-60 UV-Vis spectrophotometer (Agilent). Photoluminescence spectra were obtained with a Cary Eclipse Fluorescence Spectrophotometer (Agilent). Quartz cuvettes with an optical path length of 1 cm were used for both optical analyses.

Ellipsometry. The optical constants of the perovskites were determined from measurements using a GES5E ellipsometer from SOPRALAB with a spectral range from 1.2 to 5.5 eV. All regression analyses were performed using an in-house code.

Transmittance circular dichroism: The optical measurements were carried out in a custom-made optical set up. A white Tungsten Halogen Lamp (Ocean Optics, HL-2000-HP, Florida, USA) corrected with two filters in the UV and NIR (Edmund Optics, SCHOTT BG64, and Thorlabs, SRF11) was coupled to protected silver reflective collimator (RC08SMA-P01, Thorlabs) as light source injection. The light collection consists on another protected silver reflective collimator coupled to a spectrometer (Ocean Optics, QEPro-FL) by an optical fiber. The collimated white light beam is sent through a Glan-Thompson Calcite Polarizer (GTH10M, Thorlabs) mounted on a stepper motor rotation mount (K10CR1/M, Thorlabs). The linearly polarized light obtained is directed to a super achromatic quarter wave-plate (SAQWP05M-700, Thorlabs) mounted at $\pm\pi/4$ compared to the polarization direction on a rotation mount (ELL14, Thorlabs) to obtain a circularly polarized light beam. All the optical elements were controlled automatically by custom software (LabView NXG) to ensure the reproducibility of the measurements. The illumination area was controlled by a pinhole (SM1D12). Two dual-position sliders (ELL6, Thorlabs) were used to place a shutter and the sample in the beam path. The first one was used to measure the dark current of the spectrometer, whereas the second one was used to place the sample in the light beam. The sample was placed between a pair of 4x objectives (NA = 0.1).

Chiral emission characterization: Two laser sources (NPL41B, Thorlabs & Crylas FDSS 532-150) with peak emission at 405 nm and 532 nm were used to excite $CsPbBr_3$ and $CsPbBr_1I_2$ NCs, respectively. The PL obtained from the samples was collected through a 4X objective with 0.1 NA and collimated to a super achromatic quarter-wave plate and a Glan-Thomson polarizer. By means of a trigger controlled externally by an Arduino board (Arduino Uno), a fixed number of laser pulses were sent onto the sample to ensure both polarizations were given the same amount of energy in the excitation process. The laser signals were optically filtered using longpass band filters (FELH0450, Thorlabs for 405nm laser, BLP01-532R-25, Semrock for the 532nm laser line).

FDTD simulations.

General considerations: Finite Difference Time Domain (FDTD) simulations are performed using a commercial software (Lumerical Inc. by Ansys). The simulation reproduced a single 120 nm height and 500 nm long gammadion-like structure with 100 nm arms (width) composed of a material whose optical parameters were obtained from ellipsometry measurements (**Figure S8**) for each type of perovskite NCs. Perfectly matched layers (PML) are set in all x, y and z directions. In the case of the z-direction, the PML is placed at least half of the maximum wavelength ensure the absorption of the light source in the propagation axis avoiding back reflections and interference in the simulation region. The same PML boundary conditions were used in the x and y directions for unpolarized excitation and dipole clouds simulations.

Transmittance characterization: Two orthogonal plane wave sources with a spectral range in the visible-NIR in the x and y direction with a phase difference of $\pm\pi/2$ are used as R-CP and L-CP input light. A pair of 2D z-normal power monitors were placed to measure the transmittance and reflectance spectra for both polarizations. In the x and y directions, periodic boundary conditions were used to simulate the 2D-chiral photonic metasurface.

Unpolarized excitation: A pair of simulations with linearly polarized light at 45° and 135° to ensure the polarization does not follow any symmetry direction of the gammadion were done. These responses were added incoherently to simulate the optical response of the structure for unpolarized light. The source used was centered at 520 nm with FWHM of 40 nm, keeping the spectral region of interest for $CsPbBr_3$ NCs. A 3D-volume field profile monitor was used to record the complex electromagnetic fields to compute the optical chirality parameter $\hat{C}$ within the region of interest -500 nm < z < 500 nm at the emission frequency of 520 nm. The optical chirality was integrated along the propagation axis in the XY plane in longitudinal steps of 5 nm. The optical chirality parameter was normalized to a R-CP wave in vacuum using equation (3).

Dipolar emission: A hundred dipoles emitting at 520 nm with a FWHM of 40 nm were placed all over a single gammadion volume with random orientations and phase to ensure the incoherent interaction between the sources. The PML boundary conditions in the x and y directions ensure there is no interaction between a dipole and its mirrors images outside the unit cell, giving the results of a single gammadion emitter. The same 3-D volume field profile monitor used for unpolarized excitation was used here again to compute the optical chirality along the propagation axis. The absolute value was re-normalized, as the dipole cloud does not directly relate to a plane wave source and equation (3) does not have a direct translation to this system.

Acknowledgements

JMC and PM contributed equally to this work. This project has received funding (AEI/FEDER,-UE) from the Spanish Ministerio de Ciencia e Innovación through grants PID2019-106860GB-I00/AEI/10.13039/501100011033(HIGHN), and CEX2019-000917-S (FUNFUTURE, Spanish Severo Ochoa Centre of Excellence program) and from the Generalitat de Catalunya (2017-SGR-00488). This research was also supported by the EIC PATHFINDER OPEN project 101046489 (DYNAMO), funded by the European Union. JMC and PM acknowledge FPI fellowships (PRE2020-09411 and BES2017-080150) from MICINN cofinanced by the European Social Fund and the Ph.D. program in Materials Science from Universitat Autònoma de Barcelona. L.P. acknowledges support from the Spanish Ministerio de Ciencia e Innovación through Ramón y Cajal grant (RYC2018-026103-I) and the Spanish State Research Agency (Grant PID2020-117371RA-I00) and a grant from the Xunta de Galicia (ED431F2021/05).

Views and opinions expressed are however those of the authors only and do not necessarily reflect those of the European Union or European Innovation Council. Neither the European Union nor the granting authority can be held responsible for them.

References

[1] N. Ji, K. Zhang, H. Yang, Y.-R. Shen, *J. Am. Chem. Soc.* **2006**, *128*, 3482.
[2] A. N. Simonov, M. C. Rombach, *Opt Lett* **2011**, *36*, 115.
[3] X. Wu, L. Xu, L. Liu, W. Ma, H. Yin, H. Kuang, L. Wang, C. Xu, N. A. Kotov, *J. Am. Chem. Soc.* **2013**, *135*, 18629.
[4] M. L. Solomon, A. A. E. Saleh, L. V. Poulikakos, J. M. Abendroth, L. F. Tadesse, J. A. Dionne, *Acc. Chem. Res.* **2020**, *53*, 588.
[5] S. Lee, Y. Sun, Y. Cao, S. H. Kang, *TrAC Trends Anal. Chem.* **2019**, *117*, 58.
[6] X. Liu, Y. Lin, Y. Liao, J. Wu, Y. Zheng, *J. Mater. Chem. C* **2018**, *6*, 3499.
[7] X. Wei, J. Liu, G.-J. Xia, J. Deng, P. Sun, J. J. Chruma, W. Wu, C. Yang, Y.-G. Wang, Z. Huang, *Nat. Chem.* **2020**, *12*, 551.
[8] C. Li, X. Yang, J. Han, W. Sun, P. Duan, *Mater Adv* **2021**, *2*, 3851.
[9] G. Long, C. Jiang, R. Sabatini, Z. Yang, M. Wei, L. N. Quan, Q. Liang, A. Rasmita, M. Askerka, G. Walters, X. Gong, J. Xing, X. Wen, R. Quintero-Bermudez, H. Yuan, G. Xing, X. R. Wang, D. Song, O. Voznyy, M. Zhang, S. Hoogland, W. Gao, Q. Xiong, E. H. Sargent, *Nat. Photonics* **2018**, *12*, 528.
[10] Y. Sang, J. Han, T. Zhao, P. Duan, M. Liu, *Adv. Mater.* **2020**, *32*, 1900110.
[11] L. Protesescu, S. Yakunin, M. I. Bodnarchuk, F. Krieg, R. Caputo, C. H. Hendon, R. X. Yang, A. Walsh, M. V. Kovalenko, *Nano Lett.* **2015**, *15*, 3692.
[12] Y. Tong, E. Bladt, M. F. Aygüler, A. Manzi, K. Z. Milowska, V. A. Hintermayr, P. Docampo, S. Bals, A. S. Urban, L. Polavarapu, J. Feldmann, *Angew. Chem. Int. Ed.* **2016**, *55*, 13887.
[13] J. Shamsi, A. S. Urban, M. Imran, L. De Trizio, L. Manna, *Chem. Rev.* **2019**, *119*, 3296.
[14] J. Ye, M. M. Byranvand, C. O. Martínez, R. L. Z. Hoye, M. Saliba, L. Polavarapu, *Angew. Chem.* **2021**, *133*, 21804.
[15] "State of the Art and Prospects for Halide Perovskite Nanocrystals | ACS Nano," can be found under https://pubs.acs.org/doi/10.1021/acsnano.0c08903, **n.d.**
[16] G. Long, R. Sabatini, M. I. Saidaminov, G. Lakhwani, A. Rasmita, X. Liu, E. H. Sargent, W. Gao, *Nat. Rev. Mater.* **2020**, *5*, 423.

[17] D. Di Nuzzo, L. Cui, J. L. Greenfield, B. Zhao, R. H. Friend, S. C. J. Meskers, *ACS Nano* **2020**, *14*, 7610.
[18] J. Ma, C. Fang, C. Chen, L. Jin, J. Wang, S. Wang, J. Tang, D. Li, *ACS Nano* **2019**, *13*, 3659.
[19] Y. Liu, C. Wang, Y. Guo, L. Ma, C. Zhou, Y. Liu, L. Zhu, X. Li, M. Zhang, G. Zhao, *J. Mater. Chem. C* **2020**, *8*, 5673.
[20] Z. N. Georgieva, B. P. Bloom, S. Ghosh, D. H. Waldeck, *Adv. Mater.* **2018**, *30*, 1800097.
[21] J. Ma, H. Wang, D. Li, *Adv. Mater.* **2021**, *33*, 2008785.
[22] Y. Shi, P. Duan, S. Huo, Y. Li, M. Liu, *Adv. Mater.* **2018**, *30*, 1705011.
[23] Y.-H. Kim, Y. Zhai, H. Lu, X. Pan, C. Xiao, E. A. Gaulding, S. P. Harvey, J. J. Berry, Z. V. Vardeny, J. M. Luther, M. C. Beard, *Science* **2021**, *371*, 1129.
[24] C.-T. Wang, K. Chen, P. Xu, F. Yeung, H.-S. Kwok, G. Li, *Adv. Funct. Mater.* **2019**, *29*, 1903155.
[25] I. C. Seo, Y. Lim, S.-C. An, B. H. Woo, S. Kim, J. G. Son, S. Yoo, Q.-H. Park, J. Y. Kim, Y. C. Jun, *ACS Nano* **2021**, *15*, 13781.
[26] J. Lv, X. Gao, B. Han, Y. Zhu, K. Hou, Z. Tang, *Nat. Rev. Chem.* **2022**, *6*, 125.
[27] J. Tian, G. Adamo, H. Liu, M. Klein, S. Han, H. Liu, C. Soci, *Adv. Mater.* **2022**, *34*, 2109157.
[28] C.-L. Yu, Y.-H. Hsiao, C.-Y. Chang, P.-J. Cheng, H.-T. Lin, M.-S. Lai, H.-C. Kuo, S.-W. Chang, M.-H. Shih, *Sci. Rep.* **2020**, *10*, 7880.
[29] A. A. Maksimov, I. I. Tartakovskii, E. V. Filatov, S. V. Lobanov, N. A. Gippius, S. G. Tikhodeev, C. Schneider, M. Kamp, S. Maier, S. Höfling, V. D. Kulakovskii, *Phys Rev B* **2014**, *89*, 045316.
[30] K. Konishi, M. Nomura, N. Kumagai, S. Iwamoto, Y. Arakawa, M. Kuwata-Gonokami, *Phys. Rev. Lett.* **2011**, *106*, 057402.
[31] Z. Wang, Y. Wang, G. Adamo, J. Teng, H. Sun, *Laser Photonics Rev.* **2019**, *13*, 1800276.
[32] G. Long, G. Adamo, J. Tian, M. Klein, H. N. S. Krishnamoorthy, E. Feltri, H. Wang, C. Soci, *Nat. Commun.* **2022**, *13*, 1551.
[33] P. Liu, W. Chen, Y. Okazaki, Y. Battie, L. Brocard, M. Decossas, E. Pouget, P. Müller-Buschbaum, B. Kauffmann, S. Pathan, T. Sagawa, R. Oda, *Nano Lett.* **2020**, *20*, 8453.
[34] Y. Xia, G. M. Whitesides, *Angew. Chem. Int. Ed.* **1998**, *37*, 550.
[35] Y. Xia, J. A. Rogers, K. E. Paul, G. M. Whitesides, *Chem. Rev.* **1999**, *99*, 1823.
[36] A. Espinha, C. Dore, C. Matricardi, M. I. Alonso, A. R. Goñi, A. Mihi, *Nat. Photonics* **2018**, *12*, 343.
[37] L. Scarabelli, D. Vila-Liarte, A. Mihi, L. M. Liz-Marzán, *Acc. Mater. Res.* **2021**, *2*, 816.
[38] P. Molet, N. Passarelli, L. A. Pérez, L. Scarabelli, A. Mihi, *Adv. Opt. Mater.* **2021**, *9*, 2100761.
[39] M. Piotrowski, J. Borme, E. Carbó-Argibay, D. Sharma, N. Nicoara, S. Sadewasser, D. Y. Petrovykh, C. Rodríguez-Abreu, Y. V. Kolen'ko, *Nanoscale Adv.* **2019**, *1*, 3049.
[40] D. Vila-Liarte, M. W. Feil, A. Manzi, J. L. Garcia-Pomar, H. Huang, M. Döblinger, L. M. Liz-Marzán, J. Feldmann, L. Polavarapu, A. Mihi, *Angew. Chem. Int. Ed.* **2020**, *59*, 17750.
[41] C. Gilroy, D. J. P. Koyroytsaltis-McQuire, N. Gadegaard, A. S. Karimullah, M. Kadodwala, *Mater. Adv.* **2022**, *3*, 346.
[42] M. Schäferling, D. Dregely, M. Hentschel, H. Giessen, *Phys. Rev. X* **2012**, *2*, 031010.

[43] O. Arteaga, J. Sancho-Parramon, S. Nichols, B. M. Maoz, A. Canillas, S. Bosch, G. Markovich, B. Kahr, *Opt. Express* **2016**, *24*, 2242.
[44] C. Gilroy, S. Hashiyada, K. Endo, A. S. Karimullah, L. D. Barron, H. Okamoto, Y. Togawa, M. Kadodwala, *J. Phys. Chem. C* **2019**, *123*, 15195.
[45] S. Chen, F. Zeuner, M. Weismann, B. Reineke, G. Li, V. K. Valev, K. W. Cheah, N. C. Panoiu, T. Zentgraf, S. Zhang, *Adv. Mater.* **2016**, *28*, 2992.
[46] A. Y. Zhu, W. T. Chen, A. Zaidi, Y.-W. Huang, M. Khorasaninejad, V. Sanjeev, C.-W. Qiu, F. Capasso, *Light Sci. Appl.* **2018**, *7*, 17158.
[47] S. V. Lobanov, S. G. Tikhodeev, N. A. Gippius, A. A. Maksimov, E. V. Filatov, I. I. Tartakovskii, V. D. Kulakovskii, T. Weiss, C. Schneider, J. Geßler, M. Kamp, S. Höfling, *Phys Rev B* **2015**, *92*, 205309.
[48] E. Petronijevic, E. M. Sandoval, M. Ramezani, C. L. Ordóñez-Romero, C. Noguez, F. A. Bovino, C. Sibilia, G. Pirruccio, *J. Phys. Chem. C* **2019**, *123*, 23620.
[49] Y. Tang, A. E. Cohen, *Phys Rev Lett* **2010**, *104*, 163901.
[50] Y. Tang, A. E. Cohen, *Science* **2011**, *332*, 333.
[51] Y.-H. Kim, Y. Zhai, E. A. Gaulding, S. N. Habisreutinger, T. Moot, B. A. Rosales, H. Lu, A. Hazarika, R. Brunecky, L. M. Wheeler, J. J. Berry, M. C. Beard, J. M. Luther, *ACS Nano* **2020**, *14*, 8816.
[52] M. I. Alonso, B. Charles, A. Francisco-López, M. Garriga, M. T. Weller, A. R. Goñi, *J. Vac. Sci. Technol. B* **2019**, *37*, 062901.
[53] M. L. Brongersma, Y. Cui, S. Fan, *Nat. Mater.* **2014**, *13*, 451.
[54] P. Molet, L. K. Gil-Herrera, J. L. Garcia-Pomar, N. Caselli, Á. Blanco, C. López, A. Mihi, *Nanophotonics* **2020**, *9*, 943.
[55] J. M. Carreño, N. Passarelli, C. Otero-Martínez, L. Polavarapu, L. A. Pérez, J. S. Reparaz, M. I. Alonso, A. Mihi, *Adv. Opt. Mater.* **2022**, *10*, 2101324.
[56] D. G. Baranov, D. A. Zuev, S. I. Lepeshov, O. V. Kotov, A. E. Krasnok, A. B. Evlyukhin, B. N. Chichkov, *Optica* **2017**, *4*, 814.
[57] S. Jahani, Z. Jacob, *Nat. Nanotechnol.* **2016**, *11*, 23.
[58] E. S. A. Goerlitzer, R. Mohammadi, S. Nechayev, K. Volk, M. Rey, P. Banzer, M. Karg, N. Vogel, *Adv. Mater.* **2020**, *32*, 2001330.

Nanoimprinted 2D-chiral perovskite nanocrystal metasurfaces for circularly polarized photoluminescence

Jose Mendoza-Carreño[1⊥], Pau Molet[1⊥], Clara Otero-Martínez[2], Maria Isabel Alonso[1], Lakshminarayana Polavarapu[2] and Agustín Mihi[1]*

1 Institute of Materials Science of Barcelona ICMAB-CSIC, Campus UAB Bellaterra 08193, Spain

2 CINBIO Universidad de Vigo, Materials Chemistry and Physics Group. Department of Physical Chemistry. Campus Universitario Lagoas-Marcosende, Vigo 36310, Spain

⊥ equal contribution

* E-mail: amihi@icmab.es

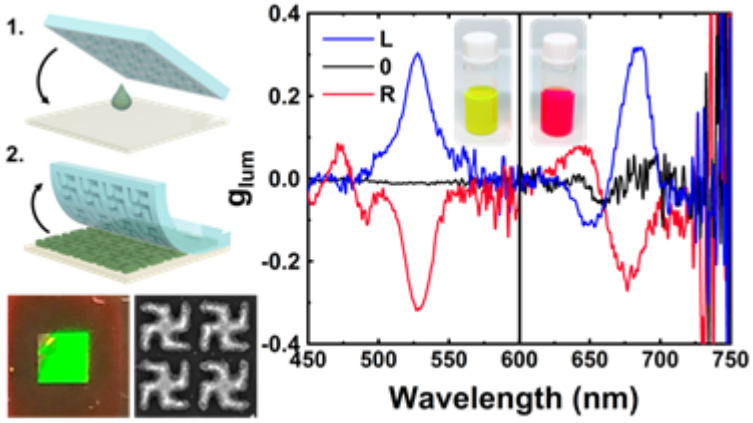

Keywords: Circularly polarized photoluminescence, chirality, nanoimprinting

Unmodified $CsPbBr_3$ and $CsPbBr_1I_2$ perovskite nanocrystals exhibit intense circularly polarized photoluminescence CPL reaching g_{lum} values up to 0.15 and 0.3 (with a high index coating) when they are nanostructured into 2D chiral metasurfaces using soft nanoimprinting lithography. The approach is scalable and leads to large areas enabling CPL production from a variety of nano-emitters.